Vehicle Charging Results from the EXCEDE III Experiment

Duane E. Paulsen, Air Force Research Laboratory, Hanscom AFB, MA

Ron Rieder, Visidyne Corporation, Burlington, MA

Ralph L. McNutt, Jr., Applied Physics Laboratory, Johns Hopkins University, Laurel, MD

Abstract: EXCEDE III was a rocket-borne, artificial aurora experiment, which was launched on 27 April 1990 from White Sands Missile Range. The payload consisted of two modules, which separated on upleg so that the sensors could observe the interaction of the electron beam with the atmosphere. We will focus on some features of the accelerator module, including the data obtained by a retarding potential analyzer (RPA) and the design and operation of the electron accelerators. The data from the RPA yields information on the vehicle potential throughout the flight. The four electron accelerators operated at 2.6 kV with a total current of 18 amperes. We will also discuss some lessons learned about the design of electron accelerators.

Introduction

EXCEDE III was an artificial aurora experiment that was flown at the White Sands Missile Range (WSMR) on 27 April 1990. It was a dual payload experiment with a sensor module carrying an extensive suite of optical sensors and an accelerator module carrying additional optical sensors, a retarding potential analyzer (RPA) and an electrostatic analyzer (ESA). The latter instruments were included to provide information about the energy distribution of the return electron current. The goal of the experiment was to excite the atmosphere with a well-characterized electron beam and to measure the resultant emissions from the atmospheric species.

The experiment was designed to minimize contamination by the rocket engine. The trajectory of the experiment was aligned with the magnetic field lines. The launch pad was near the north end of WSMR so that the launch azimuth could be about 191º, i. e. toward the south along the magnetic axis. The electron beam was directed upward along the field lines (inclination at WSMR is 61.1º. A degassant plume from the rocket engine or the payload modules would be away from the beam and below the vehicles on upleg and would become approximately orthogonal to the beam late in the downleg portion of the flight. To further alleviate contamination by the rocket exhaust the booster was separated from the payload at 95.4 s MET (mission elapsed time), about 32 seconds after burnout. The booster stayed well below the payload modules for the entire experiment. The payloads were separated at 112.4 s MET along a vector with an elevation of 23.1º and an azimuth of 286.0º with the sensor module below and to the east of the accelerator module. The modules were then oriented so that the electron beam was directed up the magnetic field lines while the primary FOV of the sensors on the sensor module intercepted the beam at a point somewhat removed from the accelerator module. A live video link showing the primary FOV and an uplink control system enabled corrections to the sensor module attitude control system (ACS) pointing program. This override capability proved to be very valuable because the separation of the two payloads happened shortly before they got into their projected orientation and the separation vector was slightly different than we had planned.

The spatial relationship between the two payload modules, the electron beam and the line-of-sight (LOS) of the primary FOV was kept nearly constant for most of the flight. As the two modules drifted further apart the intersection of the primary FOV with the electron beam moved further away from the accelerator module. As the modules moved toward apogee the practical range of the beam increases due to the creasing atmospheric density. For the upleg portion of the flight the primary FOV was always within the first few percent of the practical range of the beam. On downleg the practical range of the beam decreases with increasing density. At 100 km the primary FOV was located about 25% of the way along the practical range of the beam. At that point of the flight we initiated an attitude maneuver of the sensor module so that the primary FOV (in effect) slid down the beam.

The accelerators were operated on a 4.73 s on-2.37s off duty cycle. This was chosen to optimize the collection of data with the many instruments that were involved. Most of the instruments were free running, i. e. they were not synchronized with the accelerator duty cycle. The primary instrument, an infrared Michelson interferometer spectrometer, was synchronized with the accelerator duty cycle. The interferometer had a scan time of about two

seconds and it determined the duty cycle of the accelerator system. The accelerators started operation at 120.419s MET. The accelerators experienced numerous load faults through the first 15 seconds as expected from vacuum chamber testing. At about 136 s MET the accelerators began stable operation and underwent only occasional load faults throughout the rest of the experiment. Accelerator cycle 4, which started at 141.719 s MET, was the first complete cycle of stable operation. It also included the maximum dose, which is the portion of the experiment where the beam continued to dose the same parcel of air for the longest period of time. Dose times ranged from about 0.5 s at maximum dose to about 20 ms at apogee and about 10 ms lower down in the downleg.

We obtained excellent data with all of the sensors on the sensor module from about 136 s MET to about 263 s MET, when the accelerator module passed through the FOV. The instruments continued to function although the beam excited air was no longer in the FOV. The accelerators continued to function until 300 s MET (62 km). For the purpose of this paper we will focus on the results of the retarding potential analyzer (RPA) that was on the accelerator module. We will also include a brief description of the accelerators.

RPA Description

Our RPA was a four-grid device. There were dual entry grids that were grounded to the chassis. The entrance aperture was circular with an area of 0.32 cm^2. A retarding grid swept from +10 volts to –110 volts and then back. Each sweep took one second in one direction. The fourth grid was a suppressor grid and was also at the chassis ground. The cathode plate was held at +20 volts. The cone of acceptance had a half angle of 6.8 degrees. A logarithmic amplifier converted the measured current into an eight bit digital output that was sampled at 750 Hz. The dynamic range covered was 1 nA to 1 mA with each bit corresponding to 5.5 %. The RPA was located about 1 m from the center of the electron accelerator system with its axis aligned with the nominal axis of the electron beam.

RPA Data

The RPA started logging data at 115.4 s MET and continued until 299.3 s. A total of 185 scans were obtained. About 138 scans were obtained during accelerator cycles 4 through 23, which is the portion of the experiment where the accelerators operated as expected. Of these 66 were of sufficient quality that they could be analyzed with regression techniques. The others were not usable because the accelerators were off or there was excessive modulation caused by the attitude control system gas jets. Representative scans are shown in Figures 1 and 2.

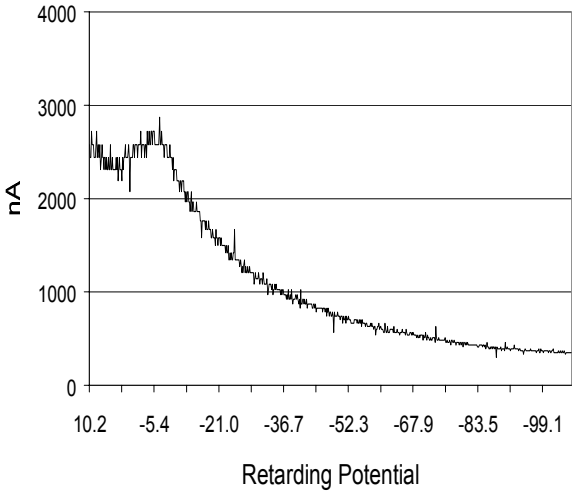

Figure 1. Scan 37 (151.6 s, 106.1 km). The scan voltage is decreasing.

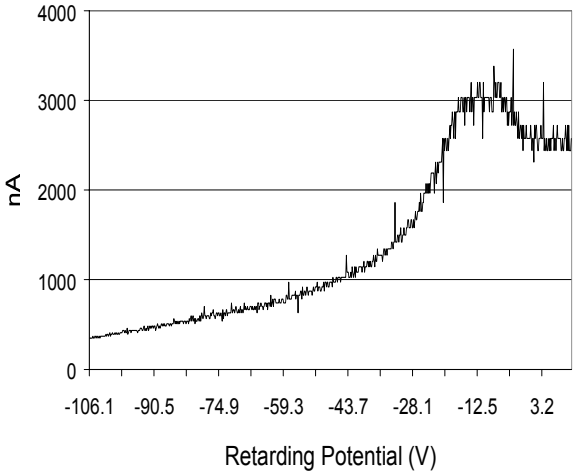

Figure 2. Scan 38 (152.6 s, 106.5 km) The scan voltage is increasing

These two scans were taken on upleg during accelerator cycle 5. They are plotted as they were recorded with the scan voltage decreasing with time in Fig. 1 and with the scan voltage increasing with time in Figure 2. Notice that in both figures there is a fairly flat peak with a rather abrupt change in the current in the neighborhood of –10 to –20 volts. Since the peak of the electron energy distribution is expected to be at about one volt, the

vehicle potential is reflected in the shoulder where the measured current begins to fall as the retarding potential becomes more negative. Clearly the distribution of electron energies has a high-energy tail that is much higher than that expected for a Maxwellian distribution. A kappa distribution (Vasyliunas, 1968) fits the measured data quite well and has been used in the analysis of the RPA data. The kappa distribution assumes a power law distribution function for the higher energy electrons with kappa representing the exponent that gives the best fit. The Maxwellian distribution is a special case of the kappa distribution where $\kappa = \infty$. Factors that are obtained by fitting the κ distribution are the vehicle potential, the mean energy of the electrons, the electron density, and the value of κ. κ values have an average value of 2.3 with a standard deviation of 0.5. They show an altitude dependence that ranges linearly from 1.9 at 115 km to 3.5 at 90 km, which means that the high-energy tail of the electron distribution is significantly enhanced at apogee. The mean value of the vehicle potential is 16 volts with a standard deviation of 5 volts. If one inspects Figs. 1 and 2 carefully there appears to be an offset in the curves of about 6 to 8 volts. We have interpreted this as hysteresis. It shows up in both the vehicle potential and the mean energy value, as one would expect. Since we have no reason to prefer one scan direction we use the average of all of the data. The value of the mean electron energy is 12 $\pm$ 4 volts. The electron densities inferred from the analysis range from about 2 x 10^7 cm^{-3} at apogee to about 1 x 10^8 cm^{-3} near 100 km. Even higher densities prevail at the center of the beam.

At various times during the flight, station-keeping requirements caused the attitude control system (ACS) of the accelerator module to activate the ACS jets. This caused nitrogen gas to be released through some combination of roll, pitch and yaw nozzles to realign the accelerator module to its desired position. The gas from the ACS jets adds to the ambient density and creates extra secondary electrons near the vehicle. The ACS system fires the gas jets at 11-12 Hz in very short pulses. The effect of these bursts of gas can be seen in Fig. 3, where we show an RPA scan taken at 172.6 s MET on upleg at 112.6 km. The current spikes rise very quickly as the nitrogen adds to the ambient neutral density and then subside as the added gas expands until it equilibrates with the ambient density. It appears that the added density provides more secondary electrons, which increase the return current to the vehicle. However, later in the flight the gas bursts cause a decrease in the RPA signal, i.e. the spikes are negative. At first this seems to be counter-intuitive. However another instrument on the accelerator module, the

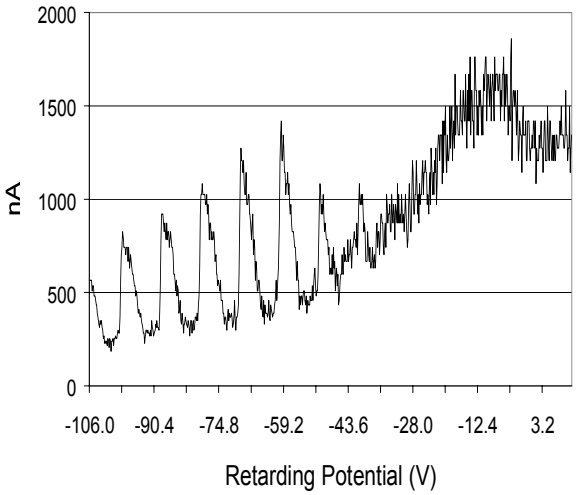

Figure 3. Scan 58 (172.6 s, 112.6 km) Positive spikes in the return current are caused by ACS jet gasses.

Electrostatic Analyzer (ESA) also shows positive and negative spikes in its measured currents. Occasionally the spikes observed by the RPA are in the opposite direction as those in the ESA measurements. When one realizes that the total return current must equal the total beam current, it is obvious that local increases in return current must be offset by corresponding decreases in other areas.

Accelerator Description and Operation

We used a simple, diode design for the electron accelerators. The anode was made of aluminum and had an aperture measuring 1 cm x 10 cm. The anode was kept at chassis ground. The cathode was made from an aluminum block. It had a V-shaped groove cut into it (See Figure 4), which focused the electrons on the anode aperture. The filament was a tungsten wire, which was spring-loaded to maintain the tension on the filament. Boron nitride insulators separated the cathode and anode. Boron nitride has many good qualities; unfortunately it absorbs gases readily and should not be used in vacuum situations. In Figure 4 we show the results of modeling the electron accelerators for a potential of 3000 V. The schematic shows the iso-potential lines and the way the electron trajectories are affected. In the orthogonal direction (parallel to the filament and the long dimension of the anode aperture) the iso-potential lines are nearly parallel and the electron

trajectories diverge very slightly. For our purposes the divergent beam worked very well. It provided a

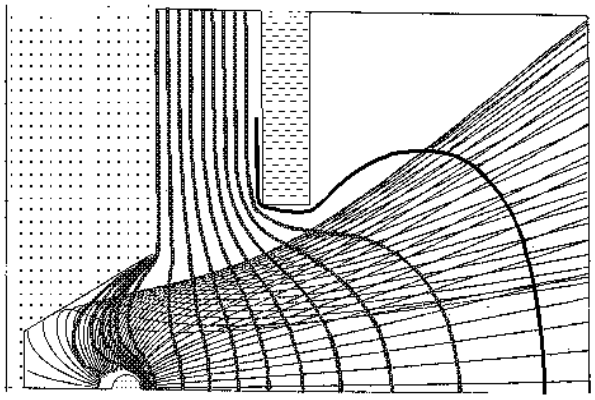

Figure 4. The V-block of the cathode is at the left, the anode in the center. This shows the modeled electron trajectories and the isopotential lines.

fairly broad beam in the far field where we were making our observations with the sensor module. It also produced a relatively low beam electron density, which help to minimize beam-plasma interactions. Banks of NiCad cells provided the accelerator power. The output voltage from the battery packs was converted to the desired accelerator voltage by a DC-DC converter operating at 730 Hz. Three separate taps provided nominal voltages of 2600, 2450 or 2300 V. Figure 5 shows the intended layout of an accelerator bay. The accelerator system consisted of two accelerator bays. We had intended to run a total of eight accelerators with an output of 5 A at 3000 V for each accelerator. However, during vacuum chamber testing at NASA's Plum Brook facility in Ohio, we learned that there were excessive load faults when we ran with eight accelerators. There was a load fault detector for each pair of accelerators. The load fault threshold was set at 19 A, which provided a safety factor of nearly two over the intended operating current for the pair of accelerators. We determined that arcing near the surface of the boron nitride insulators caused the load faults. Each time that a load fault occurred the voltage to all of the accelerators in that bay was shut down and restarted after a 0.25 s delay. Consequently the boron nitride did not degas effectively and we suffered continuous load faults. Our solution was to use only one accelerator for each load fault system. This cut the number of accelerators in half. After the load fault the high voltage came back at the next lower high voltage that was available. After two load faults in an accelerator cycle, the high voltage stayed at 2300 V.

We had also intended to run the accelerators in a perveance-limited mode. This means that the voltage and the geometry of the accelerator limit the output of the accelerator. This is usually considered the best mode for operation of accelerators in a vacuum since changes in the filament current will not affect the output current. We discovered during our chamber testing that the perveance limit, about 5 A, was easily exceeded. At the pressures we would encounter in flight that there would be significant ionization within the accelerators. This would lower the space charge effects that control the perveance limit and allow greater output currents. In the interest of greater output stability we lowered the filament voltage and, consequently the filament current so that we were below the perveance limit. We chose a current of 4.5 A for each accelerator with a total output of the accelerator system of 18 A instead of 40 A. To partially offset the lower beam current density we also lowered the beam voltage from 3000 to 2600 V. This lowered the effective beam gyroradius and increased the cross sections for excitation of the atmospheric species. By taking this conservative approach to the operation of the accelerators we were able to operate the accelerators in flight with very favorable results. After the initial clean-up period (three accelerator cycles, 21.3 s), which was characterized by frequent load faults, we achieved fairly stable operation with infrequent load faults through cycles 4 through 20 (141.7-254.4 s MET). The accelerator system started experiencing more frequent load faults at 98 km due to the increasing ambient pressure and continued to operate in a reduced capacity down to 62 km.

Summary

The EXCEDE III experiment used an electron beam operating at 2600 V and 18 A to excite the atmosphere at altitudes in the 90-115 km region. Throughout the experiment the vehicle potential was about 16 V with a standard deviation of 5 V. ACS jet gases added to the ambient neutral density, which lead to additional return current as evidenced by positive spikes in the RPA data. This effect is localized and is offset by decreases in the return current to other regions of the vehicle.

References

Vasyliunas, V. M., J. Geophys. Res. 73. 2839-2884, 1968.